Xe^+ formation following photolysis of Au–Xe: A velocity map imaging study

W. Scott Hopkins,[1] Alex P. Woodham,[1] Richard J. Plowright,[2] Timothy G. Wright,[2,a)] and Stuart R. Mackenzie[1,a)]
[1]*Department of Chemistry, University of Oxford, Physical and Theoretical Chemistry Laboratory, South Parks Road, Oxford OX1 3QZ, United Kingdom*
[2]*School of Chemistry, University of Nottingham, University Park, Nottingham NG7 2RD, United Kingdom*

(Received 14 December 2010; accepted 1 February 2011; published online 3 March 2011)

The photodissociation dynamics of Au–Xe leading to Xe^+ formation *via* the $\Xi_{1/2}$–$X^2\Sigma^+$ (v', 0) band system (41 500–41 800 cm^{-1}) have been investigated by velocity map imaging. Five product channels have been indentified, which can be assigned to photoinduced charge transfer followed by photodissociation in either the neutral or the $[Au–Xe]^+$ species. For the neutral species, charge transfer occurs *via* a superexcited Rydberg state prior to dissociative ionization, while single-photon excitation of the gold atom in Au^+–Xe accesses an (Au^+)*–Xe excited state that couples to a dissociative continuum in Au–Xe^+. Mechanisms by which charge transfer occurs are proposed, and branching ratios for Xe^+ formation *via* the superexcited Rydberg state are reported. The bond dissociation energy for the first excited state of Au^+–Xe is determined to be $\sim$9720 $\pm$ 110 cm^{-1}. © *2011 American Institute of Physics*. [doi:10.1063/1.3556944]

I. INTRODUCTION

As a result of the use of rare gas (RG) atoms in the inert messenger technique,[1] much recent experimental[2–7] and theoretical[4–13] work has concentrated on elucidating the electronic structure of coinage transition metal (TM) and RG–TM molecules, particularly in the vicinity of the strongly allowed $^2P_J \leftarrow {}^2S$ atomic transitions. Recent resonance-enhanced multiphoton ionization (REMPI) studies of the Au–RG series [RG = Ne,[5] Ar,[4] Kr,[7] and Xe (Ref. 6)] have shown that the spectroscopy of these species in the region of the Au $6^2P_J \leftarrow 6^2S$ atomic transitions is surprisingly complicated, and these complexities are borne out in the observed photodissociation dynamics.[2] Of specific interest to the present article are the spectroscopy and dynamics associated with the Au–Xe $\Xi_{1/2}$ (mixed character) state at 41 500–41 800 cm^{-1}, which was tentatively assigned as originating from the interaction between the $E^2\Sigma_{1/2}{}^+$ state associated with the Au $(^2P_{3/2})$ + Xe $(^1S_0)$ asymptote and a $^4\Pi_{1/2}$ state correlating with the higher Au $(^4P_{5/2})$ + Xe $(^1S_0)$ asymptote.[6] Interestingly, attempts to identify an analogous electronic state in the lighter members of the Au–RG series have thus far proven unsuccessful.[2]

In a recent study, we investigated the photofragmentation dynamics of Au–RG complexes in the spectral region of the Au $(^2P_{3/2})$ + RG $(^1S_0)$ dissociation threshold.[2] It was found that exciting the $\Xi_{1/2}$–$X^2\Sigma^+$ (9–13, 0) bands resulted in significant predissociation to the Au $(^2P_{1/2})$ + Xe $(^1S_0)$ threshold.[2] Excitation to the Au–Xe $\Xi_{1/2}(v' = 14)$ level, by contrast, resulted in complicated Fano spectral lineshapes and production of excited state gold atoms *via* the Au $(^2P_{1/2})$ + Xe $(^1S_0)$ and Au $(^2P_{3/2})$ + Xe $(^1S_0)$ product channels. Intriguingly, Xe^+ production was observed concomitant with $[Au–Xe]^+$ (which we use when the location of the charge is not specified, and Au^+–Xe or Au–Xe^+ when it is specified) and Au^+ production for all of the observed $\Xi_{1/2}$–$X^2\Sigma^+$ (v', 0) vibronic transitions, despite the significant mismatch in the atomic ionization energies of gold and xenon (74 409 and 97 834 cm^{-1}, respectively).[14] This is an unusual observation though not unique: REMPI studies for the rare gas–nitric oxide (RG–NO) clusters report similar observations of Xe^+ and Kr^+ formation along with the parent and cofragment ions (RG–NO^+ and NO^+, respectively).[15–21] Several mechanisms have been postulated for RG^+ production in these experiments, including multiphoton dissociation to form RG* followed by ionization,[18] and photoinduced charge transfer dissociative ionization.[15]

Here, we report the results of velocity map imaging (VMI)[22] studies of Xe^+ produced following excitation of the $\Xi_{1/2}$–$X^2\Sigma^+$ (v', 0) transitions of Au–Xe.

II. EXPERIMENTAL

The experimental apparatus employed for studying the photodissociation dynamics of Au–Xe is a purpose-built VMI time-of-flight (TOF) mass spectrometer equipped with a laser ablation cluster source, which has been described in detail previously[23] and is identical to that used in our previous Au–RG study.[2] Briefly, Au–Xe is produced by ablating a gold target (Goodfellow, 99.95%) in the presence of an argon carrier gas (BOC, >99.9%) seeded with 5% Xe. The carrier gas is admitted *via* a pulsed solenoid valve (Parker Hannifin, series 9) with the backing pressure (typically 6–8 bar) optimized for the efficient generation of small clusters. After traveling down an 18 mm cluster channel (2 mm diameter), the gas expands into vacuum. At 60 mm downstream, it is skimmed to form a molecular beam before entering the differentially pumped VMI–TOF mass spectrometer region. Here it is crossed orthogonally by the probe laser midway between

a)Authors to whom correspondence should be addressed. Electronic mail: stuart.mackenzie@chem.ox.ac.uk and Tim.Wright@nottingham.ac.uk.

the VMI repeller and extractor electrodes. The probe laser system consists of a linearly polarized, frequency-doubled, pulsed dye laser (PDL; Sirah Cobra Stretch, ~300 μJ per 8 ns pulse, $\Delta\bar{\nu} \approx 0.30$ cm^{-1}) operating with Coumarin 480 laser dye and pumped by the third harmonic of a Nd:YAG laser (Continuum, Surelite II, 10 Hz). The electric field vector of the laser is oriented so as to be parallel to the plane of the microchannel plate (MCP)/phosphor screen detector.

The instrument can operate in both in-line linear time-of-flight and velocity map imaging modes. In the former case, the mass-resolving power is sufficient to observe the different isotopologues of Au–Xe. In the VMI mode, photodissociation of Au–Xe leads to spheres of atomic fragments in the centre-of-mass frame whose expansion rate is determined by the kinetic energy release in the fragmentation process. Pulsing the rear MCP from +1200 to +1600 V during the arrival time of a given time-of-flight peak permits acquisition of signals arising from the ion of interest, while rejecting other masses. The images are recorded using a 586 × 776 pixel CCD camera, and are subsequently analyzed using a purpose built LABVIEW routine employing the Onion Peeling algorithm.[24]

III. RESULTS AND DISCUSSION

A. General comments

The Au–Xe $\Xi_{1/2}$–$X^2\Sigma^+$ (8–14, 0) REMPI spectrum as observed in the $[Au–Xe]^+$, the Xe^+, and the Au^+ mass channels is shown in Fig. 1. No hot band features are observed, which given the spectrum signal-to-noise level, are consistent with a vibrational temperature of ≤10 K. Operating in linear time-of-flight mode, the resolving power of the VMI spectrometer is such that the spectra for each Au–Xe isotopologue may be acquired individually.[2] Intriguingly, all of the spectral features observed in the $[Au–Xe]^+$ mass channel are present in both the Xe^+ and Au^+ mass channels with qualitatively similar spectral profiles. The one exception is the marked enhancement of the $v' = 14$ level observed in the Au^+ channel which was the focus of Ref. 2. The focus of the present article, however, is the observation of Xe^+ whose intensity, under the conditions employed in these studies, is a factor of 2 weaker than that of the molecular ion $[Au–Xe]^+$.

Naïvely, if an excited state of a diatomic molecule is subject to dissociation, it should not be surprising to observe the evidence in both fragment channels (provided both can be detected). We have previously shown that subsequent one-photon excitation is sufficient to ionize the excited $^2P_{1/2}$ state of Au generated in the photolysis.[2] The ionization energy of Xe, however, is ~3 eV higher than that of gold and it has many fewer low-lying excited states. Clearly, very different mechanisms must be present in the production of Au^+ and Xe^+ fragments. The $\Xi_{1/2}$–X transition is essentially a $5d^{10}6p \leftarrow 5d^{10}6s$ transition localized on the gold atom and charge transfer is therefore required to generate Xe^+.

Confirmatory evidence that the dissociation processes leading to Xe^+ and Au^+ are very different comes from the VMI images in Fig. 2, which shows $^{132}Xe^+$ and Au^+ images acquired following excitation of the $\Xi_{1/2}$–$X^2\Sigma^+$ (10, 0) transition of the Au–^{132}Xe isotopologue at 41 581.8 cm^{-1}. Several concentric rings are visible in the Xe^+ image, but only one is found in the Au^+ channel. The corresponding total kinetic energy release (TKER) spectra extracted from these images are shown in Fig. 3 from which the poor correlation between the TKER spectra observed for the two product species is obvious. The TKER peak widths observed are broader than might be expected for a diatomic dissociation. One contribution to this width is the trivial effect of the many isotopes of xenon convoluted with the kinetic energy resolution of the instrument. Other effects include the kinetic energy of the departing electron in dissociative ionization processes (see below).

Multiphoton dissociation to yield excited state Xe* or Xe^+ is unexpected. Absorption of the first photon must excite the $\Xi_{1/2}$ state, which is of mixed character and correlates with both the Au ($^2P_{3/2}$) + Xe ($^1S_0$) and Au ($^4P_{5/2}$)

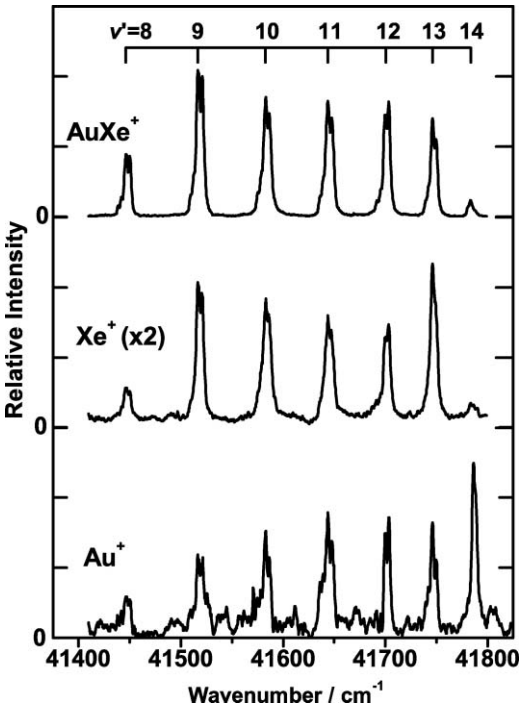

FIG. 1. The Au–Xe $\Xi_{1/2}$–$X^2\Sigma^+$ (8–14, 0) progression as observed *via* (1 + 1) REMPI in (a) the $[Au–Xe]^+$ parent ion mass channel, (b) the Xe^+ mass channel, and (c) the Au^+ mass channel (data from Ref. 2). The spectrum observed in the Xe^+ mass channel has been multiplied by a factor of 2 relative to the $[Au–Xe]^+$ channel for clarity.

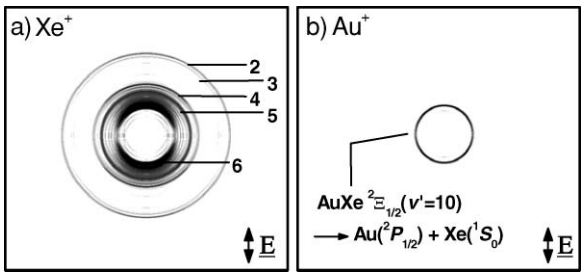

FIG. 2. VMI images recorded gating on (a) the Xe^+ ions and (b) the Au^+ following excitation of the same $\Xi_{1/2}$–$X^2\Sigma^+$ (10, 0) transition in Au−Xe at 41 581.8 cm^{-1}. Observed central spots associated with nonresonant ionization of noncomplexed Au and Xe in the molecular beam have been removed for clarity.

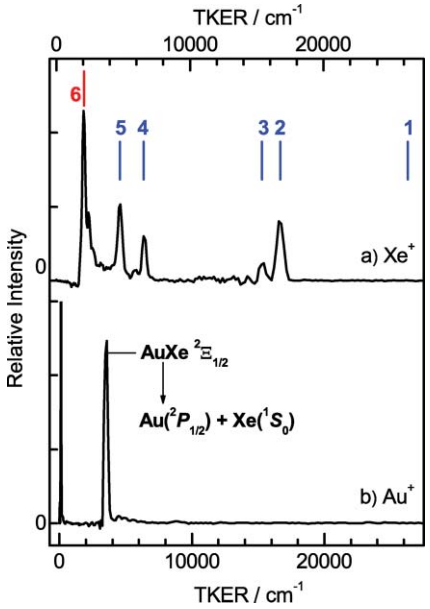

FIG. 3. The total kinetic energy release spectra extracted from the images in Fig. 2. The upper spectrum shows the TKER spectrum recorded in the Xe^+ channel, while that recorded in the Au^+ channel is shown by the below spectrum. Clearly, very different dissociation mechanisms are present in the two cases. Product channels 1–5 [blue online in (a)] show the predicted TKERs of the five accessible Xe^+ product channels at the three-photon level. Only product channel 1 is not observed. Product channel 6 (red online) is assigned to single-photon dissociation of the molecular ion (see text).

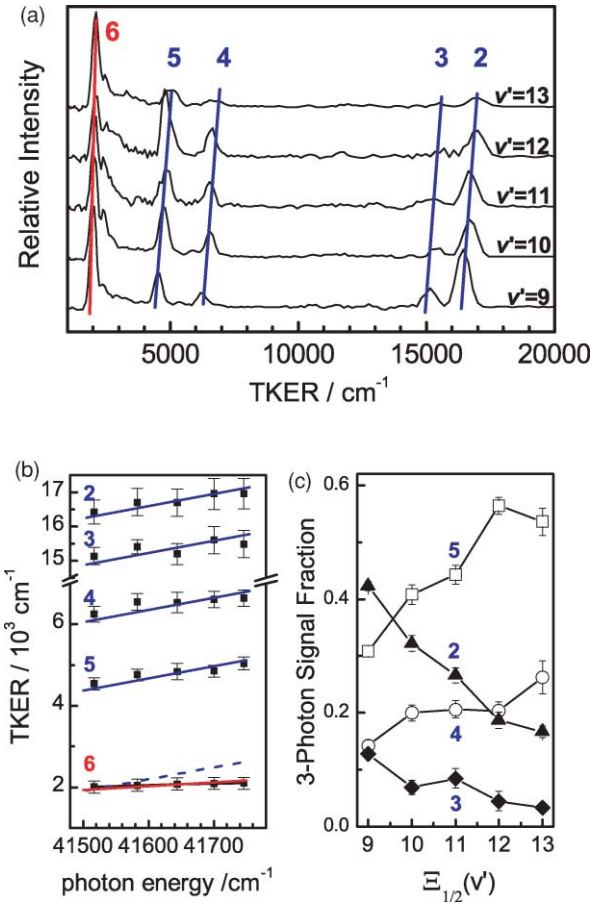

FIG. 4. (a) The TKER spectra extracted from the Xe^+ images recorded following Au–Xe photolysis *via* the $\Xi_{1/2}$–$X^2\Sigma^+$ (9–13, 0) transitions. (b) TKER peaks as a function of the excitation photon energy. Channels 2–5 have a slope of 3 (blue online) representing the expected dependence for dissociation at the three-photon level, while channel 6 has a slope of unity (red online), corresponding to single-photon dissociation. The dashed line (blue online) shows a slope of 3 for comparison purposes. (c) The fractional contributions of three-photon dissociation signal in each of the product channels 2–5.

$+$ Xe ($^1S_0$) asymptotes (and potentially has ion pair character), since the structure in the spectrum is the same as that recorded in the $[Au–Xe]^+$ mass channel. Given that this excitation is localized on the gold atom and that absorption of the second photon by gold excites Au–Xe above its first ionization energy (IE) at ~64 563 cm^{-1} (and likely also above the second and the third IEs),[25] one might expect production of the molecular ion either in the $^1\Sigma^+$ ground electronic state [correlating with Au^+ ($^1S_0$) $+$ Xe ($^1S_0$) products] or in an electronic state correlating with the low-lying $Au^+[5d^9(^2D_{5/2})6s](^5/_2,\ ^1/_2)_{2,3}$ $+$ $Xe[5p^6](^1S_0)$ asymptotes. Given that the observed $[Au–Xe]^+$ signals are approximately twice as intense as those of Xe^+, it is apparent that simple photoionization out of the $\Xi_{1/2}$ state is, in fact, the dominant process under the conditions employed, assuming similar photoionization cross sections and detection efficiencies for both species. Nevertheless, Xe^+ is observed at all wavenumbers resonant with Au–Xe $\Xi_{1/2}$–$X^2\Sigma^+$ transitions.

To investigate the photon wavenumber dependence of the peaks in the TKER spectrum, images were acquired following excitation of each of the $\Xi_{1/2}$–$X^2\Sigma^+$ (8–13, 0) transitions. For example, Fig. 4(a) shows the images obtained *via* v' = 9–13. Linear regression of the TKER peaks as a function of excitation wavenumber yields a slope that is equivalent to the number of photons required to induce dissociation [see Fig. 4(b)]. The slope of close to unity for product channel 6 [0.71 ±0.25, shown in red in Fig. 4(b)] indicates a single-photon dissociation event. The larger slope in the case of product channels 2–5 implies dissociation at the multiphoton level [for illustration, the blue lines in Fig. 4(b) correspond to a slope of 3]. In these cases, the comparatively large uncertainties in the high TKER peaks and the narrow range of photon energies accessible, preclude unambiguous assignment, by linear regression alone, of the dissociation channels or the exact number of photons involved. However, simple energy balance calculations clearly identify product channels 2–5 as arising from dissociation at the three-photon level into four of the five available Au $+$ Xe^+ channels (see notation in Fig. 3, channel 1 is not observed). In each case, the Au cofragment is produced in a quantum state that cannot be ionized with a single photon of the dissociating/ionizing laser (i.e., Au $^2D_{3/2}$ [IE = 52 973.7 cm^{-1}], $^2D_{5/2}$ [IE = 65 247.7 cm^{-1}], or $^2S_{1/2}$ [IE = 74 408.9 cm^{-1}]), which is consistent with the nonobservation of these product channels in the Au images acquired at the same wavelengths. Interestingly, as shown in Fig. 4(c), the relative branching ratios for dissociation into channels 2–5 changes notably with photolysis wavenumber, with dissociation into channels 4 and 5 increasing at the expense of channels 2 and 3 as higher vibrational levels of the $\Xi_{1/2}$ state are excited.

TABLE I. Observed Xe^+ product channels following the photolysis of Au–Xe *via* the $\Xi_{1/2}$ $v' = 10$ state at 41 581.8 cm^{-1}. Electron kinetic energy releases are predicted by energy balance calculations and reflect the Xe^+ TKER peak widths at half maximum height. Uncertainties represent ± half width at the TKER peaks at half maximum.

Product channel	Assignment	Observed TKER (cm^{-1})	Predicted TKER (cm^{-1})	Predicted electron KER (cm^{-1})
1	Au ($^2S_{1/2}$) + Xe^+ ($^2P^\circ_{3/2}$)	Not observed	26 079	
2	Au ($^2D_{5/2}$) + Xe^+ ($^2P^\circ_{3/2}$)	16 761 ± 248	16 918	225 cm^{-1}
3	Au ($^2S_{1/2}$) + Xe^+ ($^2P^\circ_{1/2}$)	15 410 ± 194	15 542	(Fixed)
4	Au ($^2D_{5/2}$) + Xe^+ ($^2P^\circ_{1/2}$)	6573 ± 157	6381	
5	Au ($^2D_{3/2}$) + Xe^+ ($^2P^\circ_{3/2}$)	4757 ± 200	4644	
6	Au ($^2D_{3/2}$) + Xe^+ ($^2P^\circ_{3/2}$)	2059 ± 167	...	2810 cm^{-1}

All dissociation channels observed are identified in Table I and the respective mechanisms responsible are discussed in more detail in Secs. III B and III C below.

B. Product channels 2–5: Dissociative ionization at the three-photon level

The three-photon excitation to yield Xe^+ products from Au–Xe must, by necessity, proceed *via* a superexcited state.[26] In principle, such a process could occur *via* a two-photon xenon-centered excitation to a molecular orbital correlating with one of the Xe [$5p^5 5d$] Rydberg states. However, given that Xe^+ formation is observed only following (gold-localized) excitation of the Au–Xe $\Xi_{1/2}$ intermediate state, a Xe-localized two-photon excitation can be ruled out. A more probable mechanism involves a process similar to the *photoinduced charge transfer* mechanism proposed by Bush *et al.* for RG–NO systems.[15]

Single-photon absorption in the 41 500–41 800 cm^{-1} region excites Au–Xe to the $\Xi_{1/2}$ state. The $\Xi_{1/2}$ state is a mixed-character state that, in part, correlates with the Au ($^5/_2$, 0)$^\circ_{5/2}$ + Xe ($^1S_0$) asymptote and thus has a Au [$5d^9(^2D_{5/2})6s6p(^3P_0{}^\circ)$] contribution to its electronic configuration. The Au configuration term symbol arises from coupling between the $^2D_{5/2}$ and $^3P_0{}^\circ$ orbital angular momenta in $(j_1, j_2)_{j\text{tot}}$ nomenclature. Absorption of the second photon can excite Au–Xe to Rydberg levels converging to the second (and/or third) ionization thresholds. Vertical excitation occurs to a Au**–Xe Rydberg state with a bond length of ~3.3 Å,[6] sufficiently short that the Rydberg orbital encompasses both Au and Xe, thus essentially preparing a Au^+–Xe ion core. Photoinduced charge transfer occurs at similar distances[27–30] and we propose that the [Au–Xe]** state switches from Au**–Xe to Au–Xe*, with the core switching from Au^+–Xe to Au–Xe^+.

A plausible mechanism for the ion core charge transfer involves coupling of molecular states correlating with the $Au^+[5d^9(^2D_{5/2})6s]$ ($^5/_2$,$^1/_2$)$_2$ + Xe [$5p^6$] ($^1S_0$) (accessed by the second photon) and the Au[$5d^{10}6s$] ($^2S_{1/2}$) + Xe^+ [$5p^5$] ($^2P^\circ_{3/2}$) asymptotes. Excitation of the Au [$5d^9(^2D_{5/2})6s6p$] center to a Rydberg state with a Au^+ [$5d^9(^2D_{5/2})6s$] ion core must generate a Rydberg *s*- or *d*-orbital to conserve angular momentum. Should the Au 6*p* electron be excited to a Rydberg *d*-orbital, then subsequent ion core switching would yield a molecular state correlating with the Xe*[$5p^5(^2P^\circ_{3/2})5d$] configuration, as the Rydberg electron is expected to be a spectator during this process. Several such Au ($^2S_{1/2}$) + Xe* asymptotes are known to lie in this energy region, the most likely for the proposed process being that associated with the Xe*[$5p^5(^2P^\circ_{3/2})5d$] $^2[^3/_2]^\circ_1$ state at 84 497 cm^{-1}, just 1300 cm^{-1} above the two-photon level.[14] The extent to which the coupling between these states is driven *via* mixing with the ion-pair (i.e., Au^-–Xe^+) states predicted to occur throughout this region is unclear.[6] Upon absorption of the third photon by the Au–Xe* species, the Rydberg electron is lost and at least some of the cationic species dissociate. It should be noted that Au^+–Xe and Au–Xe^+ are indistinguishable in our experiment. Given that the excitation energy, the AuXe dissociation energy and the photofragment internal energies are known, and the atomic/ionic TKER is measured *via* the Xe^+ product, total energy accounting can be used to determine the kinetic energy that the electron carries away. These calculations indicate that very little energy is lost (~225 cm^{-1}) as electron kinetic energy during the ionization process (see Table I).

The proposed three-photon charge transfer process is consistent with the observed image anisotropies. Figures 5(a) and 5(b) show the images recorded following excitation of the $\Xi_{1/2}$ ($v' = 9$) and $\Xi_{1/2}$ ($v' = 13$) levels, which exhibit marked differences in the anisotropies of different product channels. The interpretation of anisotropies observed following multiple-photon dissociation events has been treated theoretically by Dixon and requires some care.[31] Nevertheless, for product channels 2–5 the angular distributions are nearly isotropic, reflecting the dissociative ionization process in which the departing electron can itself carry away angular momentum as the resulting molecular state of the ion predissociates. There is a noticeable wavenumber dependence to the observed anisotropy, which increases with excitation energy. We have fit the observed angular distributions to β_2, β_4, and β_6 reflecting the likely three-photon nature, and the observed β_2 variation is shown in Fig. 5(c). At low energies (i.e., $v' = 9$) the slightly negative β_2 values are indicative of dissociation *via* a $\Sigma \rightarrow \Pi \rightarrow \Delta \rightarrow \Pi/\Phi$ mechanism, consistent with the proposed Au-centered $s \rightarrow p \rightarrow d^*$ excitation. In contrast, the extracted β_4 and β_6 parameters are approximately zero within experimental uncertainty. The origin of the variation in anisotropies with increasing photolysis

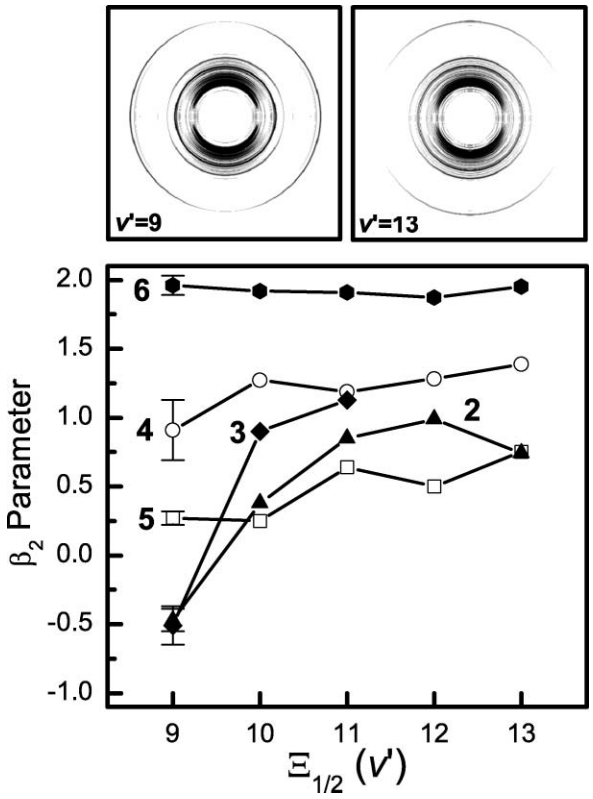

FIG. 5. (a and b) The reconstructed Xe^+ images observed following photolysis *via* the $\Xi_{1/2}$ $v' = 9$ and 13 transitions, respectively, and (c) the extracted β_2 parameters. Channels 2–5 initially exhibit low or even negative β_2 parameters for $v' = 9$, evolving to larger (more positive) values with increasing photolysis wavenumber. This effect is clear in the very outer rings in the images in (a) and (b). Product channel 6 consistently shows an angular distribution of $\beta_2 = 2$, consistent with a strongly parallel single-photon dissociation. Observed central spots associated with nonresonant ionization of noncomplexed Xe in the molecular beam have been removed for clarity.

energy is unclear, but may be associated with the changing nature of the $\Xi_{1/2}$ state, which evolves from a mixed $^4\Pi_{1/2}/^2\Sigma_{1/2}{}^+$ state to a predominantly $^2\Sigma_{1/2}{}^+$ state closer to threshold.[6]

The left hand side of Fig. 6 summarizes Xe^+ production *via* this mechanism.

C. Product channel 6: One-photon photodissociation of $[Au–Xe]^+$

The excitation wavenumber dependence of the channel 6 TKER peak suggests that it arises from a single-photon dissociation process [see 4(b)]. The most obvious candidate for such a process is dissociation of the $\Xi_{1/2}$ state. This would yield Xe ($^1S_0$) products, which cannot be detected, and is consistent with the fact that no corresponding peaks are observed in the experimental Xe^+ TKER spectrum. Given that $[Au–Xe]^+$ is readily formed by (1 + 1) REMPI of Au–Xe, photodissociation of the molecular ion is also plausible. Little, unfortunately, is known of the electronic structure of $[Au–Xe]^+$. One would expect, however, that the (1 + 1) REMPI process would yield Au^+–Xe (i.e., gold-localized charge), and thus the formation of Xe^+ from the molecular ion must also occur *via* a photoinduced charge transfer mechanism as invoked previously to account for the observations in the spectra of $Kr–O_2{}^+$ and $Kr–H_2O^+$.[29,30]

The well depth of the Au^+–Xe $^1\Sigma^+$ ground electronic state is calculated to be $D_0 = 10\,529$ cm^{-1}.[25] Single-photon excitation from Au^+–Xe $^1\Sigma^+$ ($v^+ = 0$) could access excited states correlating with the $Au^+[5d^9(^2D_{3/2})6s]$ $(^3/_2,{}^1/_2)_2$ + Xe $[5p^6]$ $(^1S_0)$ asymptote. However, charge transfer followed by dissociation to the $Au[5d^{10}6s]$ $(^2S_{1/2})$ + Xe^+ $[5p^5]$ $(^2P^o{}_{3/2})$ threshold would generate the TKER of ~6 200 cm^{-1}, ~4200 cm^{-1} larger than that observed for the product channel 6. For this mechanism to be correct, either (i) the predicted $D_0(^1\Sigma^+)$ value, obtained from very high-level *ab initio* calculations, must be in error by 40%, or (ii) single-photon absorption from the ground electronic state must result in a (forbidden) two-electron transition to higher lying molecular states followed by dissociation to another Xe^+ threshold. Neither possibility seems very likely.

The most probable explanation for the observation of channel 6 involves single-photon dissociation from low-lying ionic states correlating with the $Au^+[5d^9(^2D_{5/2})6s]$ $(^5/_2,{}^1/_2)_{2,3}$ + Xe $[5p^6]$ $(^1S_0)$ asymptotes. Such states could be prepared *via* autoionization of the Au–Xe** superexcited state generated by the mechanism described in Sec. III B, or by removal of the 6*p* electron from the Au $[5d^9(^2D_{5/2})6s6p]$ $(^3P^o{}_0)$ contribution to the $\Xi_{1/2}$ state. Assuming a potential energy well depth similar to that of the ionic ground state, an excited ionic state correlating with the $Au^+[5d^9(^2D_{5/2})6s]$ $(^5/_2,{}^1/_2)_2$ + Xe $[5p^6]$ $(^1S_0)$ asymptote would lie at ~80 000 cm^{-1} (i.e., ~3000 cm^{-1} below the two-photon energy level). Such an assumption is reasonable given that both the Au $5d^{10}$ ground state and $5d^96s$ excited state are spherically symmetric and are thus expected to exhibit similar potential well depths when bound to Xe. Importantly, this excited state is metastable with respect to the ground state, and (gold-localized) single-photon absorption can access molecular ion states correlating with the $Au^+[5d^86s^2]$ + Xe$[5p^6]$ or $Au^+[5d^96p]$ + Xe$[5p^6]$ configurations, the most likely candidate for which being gold-localized excitation to an ionic state correlating with the Au^+ $5d^9(^2D_{5/2})6p$ $(^5/_2,{}^1/_2)_2{}^\circ$ + Xe $5p^6$ $(^1S_0)$ threshold (analogous to the Au^+ $5d^9(^2D_{5/2})6s$ $(^5/_2,{}^1/_2)_2 \rightarrow 5d^9(^2D_{5/2})6p$ $(^5/_2,{}^1/_2)_2{}^\circ$ transition at 48 013.746 cm^{-1}).[14] This excitation would also serve to promote Au^+–Xe above the first five thresholds leading to Xe^+ formation, and, in particular, to the region of the bound states associated with the Au $(^2D_{3/2})$ + Xe^+ $(^2P^o{}_{1/2})$ asymptote and dissociative continuum associated with the Au $(^2D_{3/2})$ + Xe^+ $(^2P^o{}_{3/2})$ asymptote (see the right hand side of Fig. 6). Coupling between the $Au^+(J = 2)$–$Xe(^1S_0)$ and $Au(^2D_{3/2})$–$Xe^+(^2P^o{}_{3/2,1/2})$ potential energy curves could then induce charge transfer and dissociation to the $Au(^2D_{3/2})$ + $Xe^+(^2P^o{}_{3/2})$ threshold. The predicted TKER for this process is in very good agreement with that observed for product channel 6 which would imply that the electron emitted during the autoionization carries away 2800 cm^{-1}. Figure 6 (right) provides a schematic diagram summarizing this mechanism.

Further support for such a mechanism is provided by the observed product angular distributions. Photoinduced charge transfer to a dissociative state is expected to be very fast and the observed product angular distributions should, therefore,

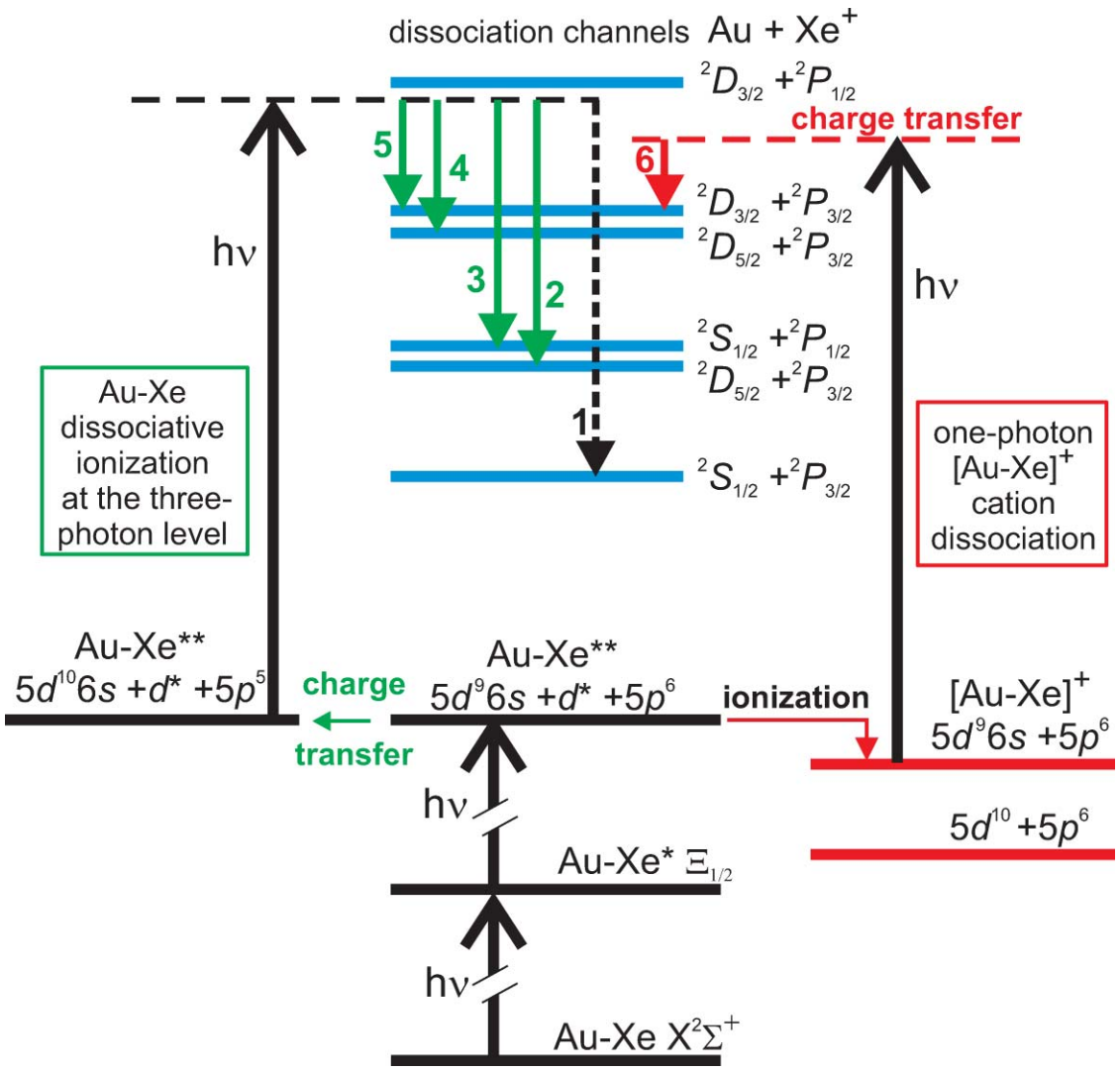

FIG. 6. Summary of Au–Xe dissociation channels observed in the Xe^+ channel. (Right) Excitation out of the $\Xi_{1/2}$ state leads to direct ionization in a (1 + 1) REMPI process. Subsequent one-photon dissociation of the molecular cation $[Au–Xe]^+$, generates Xe^+ in channel 6. (Left) Excitation out of the $\Xi_{1/2}$ state generates a superexcited Au–Xe** state which undergoes charge transfer, switching the ion core configuration to $Au(5d^{10}6s)–Xe^+(5p^5)$ with the charge localized on the Xe. Absorption of a further photon leads to dissociative ionization at the three-photon level into Au + Xe^+ product channels 2–5 as indicated.

reflect the parallel or perpendicular nature of the electronic transition. As can be seen in Fig. 5, product channel 6 consistently (within error) displays extreme angular distributions of $\beta_2 = 2$, implying that photodissociation follows a parallel transition, which is consistent with a gold-localized excitation *via* the Au^+ $(^5/_2,^1/_2)_2 \rightarrow 2$ transition.

Finally, given the above mechanism, we can extract more information from the observed TKER peak associated with product channel 6. Closer examination of the channel 6 TKER peak [Fig. 4(a)] shows that it is asymmetric and degraded to high TKER, consistent with the formation of the molecular ion in several vibrational states. If we identify the sharp onset of the TKER peak at 2040 cm^{-1} with the $v = 0$ state of the ion, with a Franck–Condon envelope of decreasing probabilities extending to higher TKER, we can extract a (Au^+)*–Xe dissociation energy, $D_0 = 9720 \pm 110$ cm^{-1}, a value which is consistent with that calculated for the ground electronic state.[25]

IV. CONCLUSIONS

Xe^+ photofragments generated following resonant excitation *via* the $\Xi_{1/2}$–$X^2\Sigma^+$ (v', 0) band system in Au–Xe have been investigated using velocity map imaging. Energy balance calculations facilitate the assignment of the five observed product channels, four of which arise *via* photoinduced charge transfer in a superexcited Rydberg state at the two-photon level prior to dissociative ionization at the three-photon level. The fifth product channel may be assigned to single-photon dissociation of an excited state of the molecular ion formed *via* (1+1) REMPI of Au–Xe. Photodissociation of Au^+–Xe to form Xe^+ also occurs *via* a photoinduced charge transfer mechanism. Asymmetry of the TKER peak associated with product channel 6 indicates that photolysis occurs *via* excitation from several vibrational levels associated with the excited Au^+–Xe electronic state, with the most intense TKER feature likely being associated with the $v = 0$ level. The bond

dissociation energy for this excited ionic state is derived as $\sim 9720 \pm 110\ cm^{-1}$.

ACKNOWLEDGMENTS

Funding for this research was provided by the Engineering and Physical Sciences Research Council (EPSRC, Grant No. EP/C012070) and S.R.M. is further grateful to the EPSRC for his Advanced Research Fellowship (Grant No. EP/C01202X). W.S.H. acknowledges funding from the Ramsay Memorial Fellowships Trust in the form of a Ramsay Memorial Fellowship. T.G.W. and R.J.P. are grateful for support from the EPSRC (Grant No. GR/S78599/02).

[1]G. Gregoire and M. A. Duncan, J. Chem. Phys. **117**, 2120 (2002).
[2]W. S. Hopkins, A. P. Woodham, R. J. Plowright, T. G. Wright, and S. R. Mackenzie, J. Chem. Phys. **132**, 214303 (2010).
[3]A. M. Knight, A. Stangassinger, and M. A. Duncan, Chem. Phys. Lett. **273**, 265 (1997).
[4]R. J. Plowright, V. L. Ayles, M. J. Watkins, A. M. Gardner, R. R. Wright, T. G. Wright, and W. H. Breckenridge, J. Chem. Phys. **127**, 204308 (2007).
[5]R. J. Plowright, A. M. Gardner, C. D. Withers, T. G. Wright, M. D. Morse, and W. H. Breckenridge, J. Phys. Chem. A **114**, 3103 (2010).
[6]R. J. Plowright, M. J. Watkins, A. M. Gardner, C. D. Withers, T. G. Wright, and W. H. Breckenridge, Phys. Chem. Chem. Phys. **11**, 1539 (2009).
[7]R. J. Plowright, M. J. Watkins, A. M. Gardner, T. G. Wright, W. H. Breckenridge, F. Wallimann, and S. Leutwyler, J. Chem. Phys. **129**, 154315 (2008).
[8]N. C. Bera, I. Bhattacharyya, and A. K. Das, Spectrochim. Acta, Part A **67**, 894 (2007).
[9]F. Cargnoni, T. Kus, M. Mella, and R. J. Bartlett, J. Chem. Phys. **129**, 204307 (2008).
[10]X. Li, X. Cao, J. H. Jiang, and Y. F. Zhao, Eur. Phys. J. D **55**, 87 (2009).
[11]X. Y. Li, C. Xue, and Y. F. Zhao, Theor. Chem. Acc. **123**, 469 (2009).
[12]T. G. Wright, M. J. Watkins, R. J. Plowright, and W. H. Breckenridge, Chem. Phys. Lett. **459**, 70 (2008).
[13]T. Xiao-Fei, Y. Chuan-Lu, A. Yi-Peng, W. Mei-Shan, M. Xiao-Guang, and W. De-Hua, J. Chem. Phys. **131**, 244304 (2009).
[14]Y. Ralchenko, A. E. Kramida, J. Reader, and NIST ASD Team (2008), NIST Atomic Spectra Database (version 3.1.5), National Institute of Standards and Technology, Gaithersburg, MD, 2009, Available: http://physics.nist.
[15]A. M. Bush, J. M. Dyke, P. Mack, D. M. Smith, and T. G. Wright, Chem. Phys. **223**, 239 (1997).
[16]S. D. Gamblin, S. E. Daire, J. Lozeille, and T. G. Wright, Chem. Phys. Lett. **325**, 232 (2000).
[17]J. C. Miller, J. Chem. Phys. **86**, 3166 (1987).
[18]J. C. Miller, J. Chem. Phys. **90**, 4031 (1989).
[19]B. Wen, H. Meyer, V. L. Ayles, A. Musgrave, D. E. Bergeron, J. A. E. Silber, and T. G. Wright, Phys. Chem. Chem. Phys. **10**, 375 (2008).
[20]P. Mack, J. M. Dyke, D. M. Smith, T. G. Wright, and H. Meyer, J. Chem. Phys. **109**, 4361 (1998).
[21]P. Mack, J. M. Dyke, and T. G. Wright, J. Chem. Soc., Faraday Trans. **94**, 629 (1998).
[22]A. Eppink and D. H. Parker, Rev. Sci. Instrum. **68**, 3477 (1997).
[23]W. S. Hopkins, S. M. Hamilton, P. D. McNaughter, and S. R. Mackenzie, Chem. Phys. Lett. **483**, 10 (2009).
[24]G. M. Roberts, J. L. Nixon, J. Lecointre, E. Wrede, and J. R. R. Verlet, Rev. Sci. Instrum. **80**, 053104 (2009).
[25]W. H. Breckenridge, V. L. Ayles, and T. G. Wright, J. Phys. Chem. A **112**, 4209 (2008).
[26]R. L. Platzman, Radiat. Res. **17**, 419 (1962).
[27]D. A. Copeland and C. L. Tang, J. Chem. Phys. **65**, 3161 (1976).
[28]L. F. Errea, L. Mendez, and A. Riera, J. Chem. Phys. **79**, 4221 (1983).
[29]M. F. Jarrold, L. Misev, and M. T. Bowers, J. Chem. Phys. **81**, 4369 (1984).
[30]H. S. Kim, C. H. Kuo, and M. T. Bowers, J. Chem. Phys. **93**, 5594 (1990).
[31]R. N. Dixon, J. Chem. Phys. **122**, 194302 (2005).